Materials & Design 233 (2023) 112273

Contents lists available at ScienceDirect

Materials & Design

journal homepage: www.elsevier.com/locate/matdes

New insights into the molecular structure and dynamics of a recyclable and ionically crosslinked carboxylated nitrile rubber (XNBR)

Saul Utrera-Barrios [a], Reyes Verdugo Manzanares [a], Antonio Mattia Grande [b], Raquel Verdejo [a], Miguel Ángel López-Manchado [a,*], Marianella Hernández Santana [a,*]

[a] Institute of Polymer Science and Technology (ICTP), CSIC, Juan de la Cierva 3, 28006 Madrid, Spain
[b] Department of Aerospace Science and Technology, Politecnico di Milano, Milano, via la Masa 34, 10156 Milano, Italy

ARTICLE INFO

Keywords:
Nitrile rubber
Recycling
Ionic network
Molecular dynamics
Circular economy

ABSTRACT

Ionic crosslinking offers a route to rubber reprocessability due to ion pairs' dynamism, with recent studies focusing on tensile properties recovery. However, this research aims to provide, for the first time, a comprehensive overview of the recyclability of carboxylated nitrile rubber (XNBR), spotlighting changes in molecular dynamics through multiple recycling cycles beyond tensile tests. A uniquely recyclable XNBR, incorporating ZnO as a multifunctional additive, was designed alongside a simple, scalable, two-step recycling process. Evidence of the delicate balance between crosslink density and molecular entanglements that affects the dynamics of the recycled material was found. Recycling also restricts the molecular dynamics near ionic domains; attributed to a higher crosslink density (from 3.69×10^{-5} mol cm^{-3} in the pristine sample to 6.00×10^{-5} mol cm^{-3} after the third cycle), caused by a decreased ionic clusters size (aggregation number drops from 12.2 to 6.9). Remarkably, negligible differences (< 10%) in compressive fatigue behavior and an enhanced chemical resistance in different solvents (up to 350% increase in motor oil) were also observed, ensuring suitable performance in conditions closer to service. Overall, this study demonstrates the feasibility of XNBR recycling and provides a broad understanding of this material at the molecular level.

1. Introduction

The carboxylation of elastomers is a well-known strategy in the rubber industry [1]. The goal is to impart improved functionalities such as abrasion, tear, and chemical resistance to the rubber chain [2]. One of the most common carboxylated elastomers is carboxylated nitrile rubber (XNBR), a terpolymer obtained from the copolymerization of acrylonitrile, butadiene, and carboxylic acid (mainly acrylic acid or methacrylic acid) [3]. The incorporation of this third monomer allows these materials to react with metal oxides, metal peroxides, salts, and thiolates, among others [4–7], resulting in the formation of carboxylic salts that behave as ionic crosslinks [8]. These carboxylic salts tend to associate as multiplets and clusters following an accepted structure known as the Eisenberg Model [9,10]. Multiplets consist of six to eight dipole ions associated to form larger structures, which disperse in the elastomeric matrix without forming a separate phase [11]. Clusters are considered aggregates formed by such multiplets and trapped chains. This association is caused by electrostatic interactions and is affected by the elastic shrinkage forces of rubber macromolecules. The restricted mobility of elastomer chains in the vicinity of ionic groups results in the formation of a hard phase immersed in a polar matrix [12]. This heterogeneity results in a distinct "ionic domain" with its own "glass/ionic transition". The release of polymer chains during long-range hopping of ions [13] leads to an increase in the molecular motion of the system, which is a reversible process [14].

Unlike the common covalent crosslinks formed during conventional vulcanization with sulfur/accelerant systems or peroxides, ionic crosslinks are dynamic, and cluster formation is responsible for the enhanced physical properties of ionic elastomers even without the addition of fillers [4,14–18]. Their dynamic character allows them to be reprocessable by applying medium to high temperatures, such as a thermoplastic elastomer (TPE) [19,20]. This has resulted in a substantial change from an environmental point of view. It is well known that crosslinked rubbers cannot be reprocessed using non-dynamic covalent systems. Thus, the use of dynamic networks in elastomeric materials is of great scientific, industrial, and environmental importance [21–23].

* Corresponding authors.
E-mail addresses: lmanchado@ictp.csic.es (M.Á. López-Manchado), marherna@ictp.csic.es (M. Hernández Santana).

https://doi.org/10.1016/j.matdes.2023.112273
Received 16 May 2023; Received in revised form 15 August 2023; Accepted 22 August 2023
Available online 28 August 2023

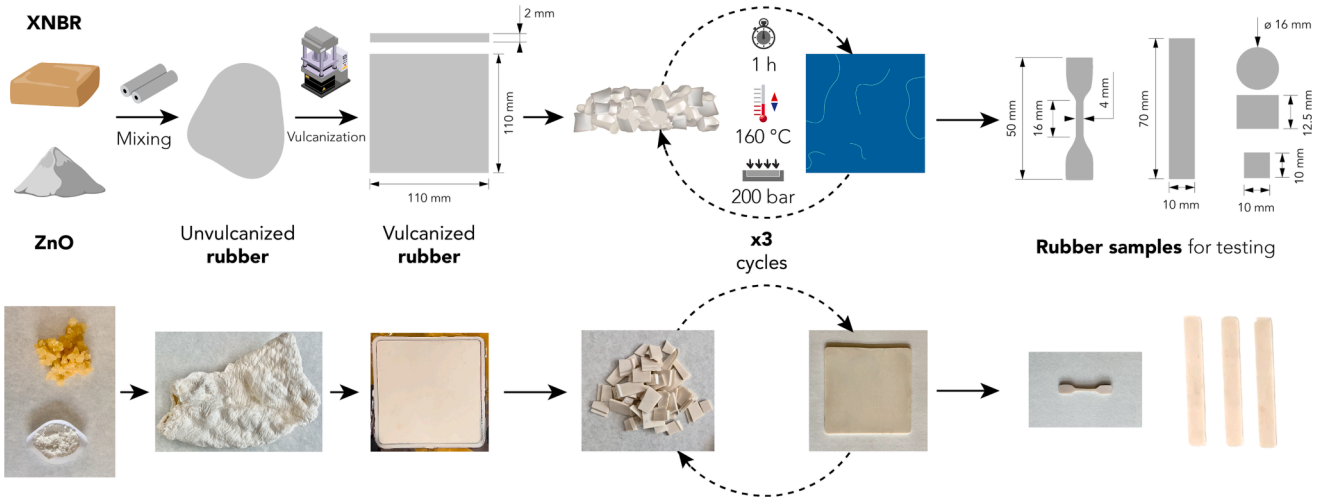

Fig. 1. Recycling protocol scheme.

Various authors have explored the dynamic nature of ionic elastomers [24–29]. Das and Naskar [25] described a sacrificial network of XNBR crosslinked by metal–ligand coordination complexes, based on zinc nitrate ($Zn(NO_3)_2$) and zinc chloride ($ZnCl_2$), which exhibited good tensile strength, recyclability, and potential for O-ring applications. The authors found that the dynamic character and tensile performance of the compounds were dependent on the nature of the counterions and ligand-to-metal ratio. They suggested that the weak and dynamic zinc-carboxylate coordination bonds formed by $Zn(NO_3)_2$ and XNBR make them more suitable for recycling than the stiffer $ZnCl_2$-based crosslinked compounds. Recently, Zainol et al. [26] reported crosslinking of commercial XNBR with zinc thiolate ($C_{10}H_6O_4S_2Zn$, ZT). The reversible nature of these ionic crosslinks provides self-healing, weldability, and recyclability to the prepared materials. The amount of ZT was varied, and the evidence of ionic crosslinks was determined by increasing the curing torque. The study revealed that the material could recover 98 % of its initial tensile properties under a thermal protocol at 150 °C for 10 min, even after being reprocessed and recycled three times. XNBR/ZT also exhibited excellent weldability and high potential for repairing existing rubber products used in heavy engineering applications. Chatterjee et al. [27] and Salaeh et al. [28] presented TPE using XNBR as elastomeric phase and polyamide 12 (PA12) and poly(vinylidene fluoride) (PVDF) as thermoplastic phase, respectively, and zinc oxide (ZnO) as crosslinking agent. They reported 100 % reprocessability of the developed materials. Recently, Das et al. [29] investigated an XNBR network crosslinked by biologically derived coordination complexes, resulting in room-temperature self-healing properties, high tensile strength, stretchability, and recyclability. The complexes were synthesized using nickel nitrate ($Ni(NO_3)_2$) and $Zn(NO_3)_2$ metal salts in combination with l-cysteine amino acids. Different analytical techniques confirmed the successful formation of these metal-cysteine complexes. Specifically, the Zn-cysteine complex-cured XNBR compound demonstrated the best overall performance with extreme stretchability, tensile strength of 3.8 MPa, remarkable healing performance of 89.5 %, and recycling efficiency of 82 %. These studies highlight the potential of Zn-based coordination complexes for the production of sustainable rubber compounds.

It is important to note that, as in the examples above, the vast majority of studies in the area of the reprocessability/recycling of ionic elastomers are highly focused on the analysis of mechanical recovery. Only a few authors have attempted to go beyond tensile test evaluation to assess the changes in the ionic phase of this type of material with temperature (but without a focus on recyclability) using different advanced techniques such as Dynamic Mechanical Analysis (DMA) [14], ^{1}H low-field Nuclear Magnetic Resonance (NMR) [30], and Small-Angle X-ray Scattering (SAXS) [31]. However, to the authors best knowledge, no comprehensive study has analyzed the changes that occur in the material network through different recycling cycles.

The aim of this study is to answer a critical question: can the dynamic and reversible nature of ionic elastomers retain the characteristics of their network after each recycling cycle? The answer to this question is crucial for understanding the true potential of these materials for achieving sustainable rubber. For this purpose, two key design fronts were addressed: material composition and recycling process. A uniquely recyclable XNBR was designed, using only a single metal oxide (ZnO). This multifunctional design accomplishes three critical roles, serving as a crosslinking agent, reinforcing filler, and processing aid. Complementarily, a straightforward recycling methodology, consisting of just two simple steps (cutting and (re)molding), was developed. The simplicity of this process design not only fosters ease of execution but importantly ensures scalability, a prevailing challenge in the recycling of elastomeric materials. Subsequently, the samples were recycled up to three times and the material obtained after each recycling cycle was systematically evaluated for the first time at the molecular level using DMA, X-ray Diffraction (XRD), and Broadband Dielectric Spectroscopy (BDS). The changes in the molecular dynamics with recycling cycles were correlated with the morphology and physical (crosslink density), mechanical (tensile and compressive fatigue), and chemical (solvent resistance) properties of the rubber.

2. Experimental section

2.1. Materials

XNBR (KRYNAC X 750) cold polymerized, non-staining stabilized, consisting of 27 wt% acrylonitrile content and 7 wt% carboxyl groups, was kindly provided by Arlanxeo. Merck supplied ZnO as a crosslinking agent, and toluene (ACS reagent, $\geq$ 99.5 %) was used to assess the crosslink density and chemical resistance, together with motor oil and gasoline 95 from Repsol (Spain). All the products were used without further purification.

A single recipe based on 100 parts per hundred rubber (phr) XNBR and an excess of 10 phr of ZnO was prepared and identified as 10ZnO. This compound was chosen based on a prior optimization study conducted by the authors [12,32], which evaluated different ZnO contents and determined that the 10ZnO composition exhibited the most favorable mechanical behavior for two primary reasons. The first is the complete neutralization of the carboxyl groups in XNBR, given the challenges associated with dispersing ZnO agglomerates during traditional rubber mixing. Secondly, the semi-reinforcing effect of ZnO [33],

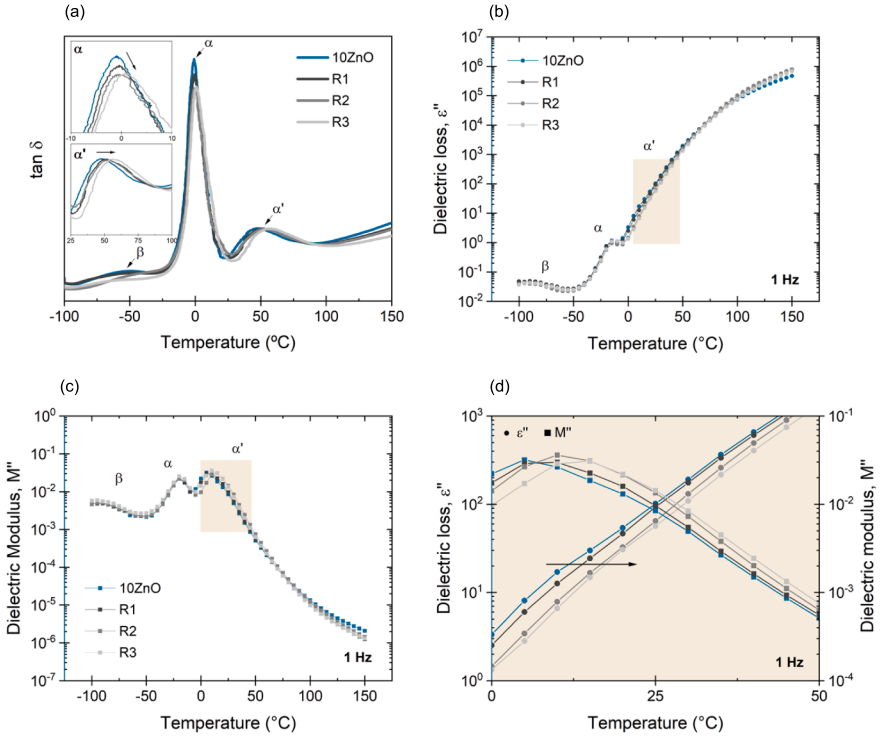

Fig. 2. (a) *tan*(δ) vs temperature by DMA. (b) Dielectric loss, ε'' and (c) modulus M'' vs temperature at 1 Hz, and (d) inset of ionic relaxation with recycling cycles by BDS.

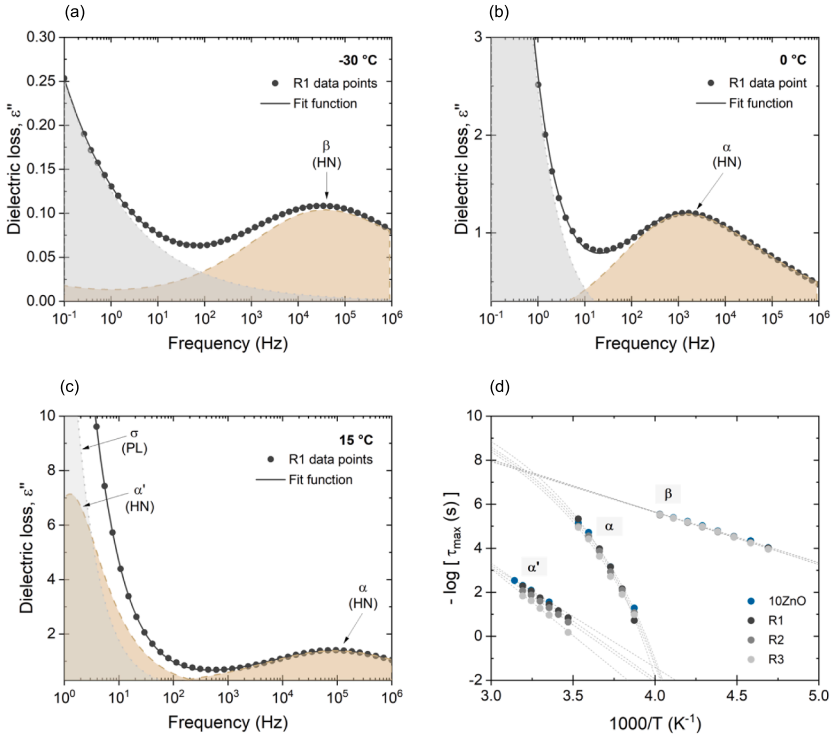

Fig. 3. HN– (dash) and PL-function (dots) fittings for (a) β, (b) α and (c) α' relaxations for R1. (d) Activation diagram for pristine 10ZnO and each recycled sample, where the dashed lines represent the fit by VFTH-function for α relaxation and by Arrhenius function for β and α'.

Table 1
VFTH and Arrhenius fitting parameters for each dielectric relaxation.

Parameter	10ZnO	R1 (Recycled 1)	R2 (Recycled 2)	R3 (Recycled 3)
β relaxation				
E_a(kJ/mol)	45 ± 1	44 ± 1	45 ± 1	46 ± 1
α relaxation				
B	1574 ± 29	1466 ± 45	1657 ± 40	1699 ± 54
T_0(K)	204 ± 1	210 ± 2	203 ± 2	202 ± 2
D	7.7 ± 0.1	7.0 ± 0.3	8.2 ± 0.3	8.4 ± 0.3
m	93 ± 4	101 ± 4	88 ± 3	86 ± 2
α' relaxation				
E_a(kJ/mol)	85 ± 2	101 ± 2	100 ± 3	116 ± 5

Table 2
Mooney-Rivlin constants and crosslink density values.

Sample	$2C_1$	$2C_2$	$\upsilon_{Mooney-Rivlin}$ ($\times 10^{-4}$ mol cm^{-3})	$\upsilon_{swelling}$ ($\times 10^{-5}$ mol cm^{-3})
10ZnO	0.31 ± 0.01	0.91 ± 0.05	1.25 ± 0.02	3.69 ± 0.03
R1 (Recycled 1)	0.45 ± 0.06	1.23 ± 0.12	1.83 ± 0.24	4.75 ± 0.12
R2 (Recycled 2)	0.49 ± 0.05	1.15 ± 0.10	1.96 ± 0.21	5.85 ± 0.97
R3 (Recycled 3)	0.55 ± 0.06	1.04 ± 0.15	2.22 ± 0.24	6.00 ± 0.58

which can improve the mechanical properties of the vulcanizate beyond its saturation point.

2.2. Processing

2.2.1. Compounding

A two-roll mill (MGN-300S, Comerio Ercole S.P.A.) was used to mix both ingredients for 25 min at room temperature following a previously established mixing protocol [12]. Curing curves were determined using a moving die rheometer (MDR 2000, Alpha Technologies) with a 0.5° oscillation arc and 1.7 Hz frequency for 60 min. Subsequently, the compound was vulcanized by compression molding using a hydraulic press (TP300, Gumix) according to the curing time (t90) at 160 °C and 200 bar. The material was then cooled inside the press, maintaining the selected pressure, and circulating cold water for 5 min to avoid bubbles in the vulcanized product. The final samples were cut for each characterization technique at least 24 h after molding.

2.2.2. Recycling protocol

Once vulcanized sheets have been obtained, the first step in the recycling process is to shred the material into small pieces (approximately 1 cm^2 area), which increases its surface area and makes it easier to reprocess. The small pieces were then placed in a hydraulic hot press and heated to 160 °C at 200 bar for 1 h. This process is identified as one recycling cycle (R1), which causes the material to "fuse" and form a new solid sheet. After cooling, the methodology was repeated for up to three cycles (R2 and R3). Each time the material was recycled, its properties were fully determined. This approach proved efficient and produced high-quality sheets. Fig. 1 shows a schematic of the mixing, vulcanization, and recycling protocol of the prepared sample.

2.3. Characterization

2.3.1. Dynamic mechanical analysis (DMA)

A DMA analyzer (Q800, TA Instruments) was used to perform temperature sweeps from − 100 °C to 150 °C in tension mode at 15μ m amplitude, 1 Hz, and a heating rate of 2 °C min^{-1}.

2.3.2. Broadband dielectric Spectroscopy (BDS)

Frequency sweeps ranging from 10^{-1} to 10^6 Hz were performed on a high-resolution dielectric analyzer (ALPHA, Novocontrol Technologies) from − 100 to 150 °C in increments of 5 °C. The complex dielectric function in the frequency domain ($\varepsilon^*(\omega)$) was obtained as expressed in equation (1) [34,35]:

$$\varepsilon^*(\omega) = \varepsilon'(\omega) - i\varepsilon''(\omega) \tag{1}$$

where $\varepsilon'(\omega)$ is the real part and is proportional to the energy stored reversibly in the system and $\varepsilon''(\omega)$ is the imaginary part and is proportional to the dissipated energy (also known as dielectric loss).

For a supplemental visualization of the effects over the complex dielectric function, the reciprocal of the complex permittivity ($1/\varepsilon^*(\omega)$), known as the complex electric modulus ($M^*(\omega)$), can be used and is expressed as seen in equation (2):

$$M^*(\omega) = M'(\omega) + iM''(\omega) = \frac{\varepsilon'(\omega)}{(\varepsilon'(\omega))^2 + (\varepsilon''(\omega))^2} + i\frac{\varepsilon''(\omega)}{(\varepsilon'(\omega))^2 + (\varepsilon''(\omega))^2} \tag{2}$$

Analysis of the dielectric spectra and each dielectric relaxation process requires the use of different model functions. One of the most general functions is the Havriliak-Negami function (HN-function), according to equation (3):

$$\varepsilon^*_{HN}(\omega) = \varepsilon_\infty + \frac{\Delta\varepsilon}{(1 + (i\omega\tau_{HN})^\alpha)^\beta} \tag{3}$$

where α and β are two parameters related to the symmetric and asymmetric broadening of the complex dielectric function, respectively, with $0 < \alpha$ and $\alpha\beta \leq 1$, $\Delta\varepsilon = \varepsilon_0 - \varepsilon_\infty$ is the dielectric strength, where ε_0 is the relaxed ($\omega = 0$) and ε_∞ the unrelaxed ($\omega = \infty$) dielectric constant values, respectively; and, finally, τ_{HN} is the HN relaxation time, related to the position of maximal loss in the HN-function. α and β are also related to the overall position of each maximal loss ($\tau_{max} = 1/\omega_{max}$), according to equation (4):

$$\tau_{max} = \tau_{HN}\left[\sin\left(\frac{\alpha\pi}{2+2\beta}\right)\right]^{-\frac{1}{\alpha}}\left[\sin\left(\frac{\alpha\beta\pi}{2+2\beta}\right)\right]^{\frac{1}{\alpha}} \tag{4}$$

Typically, different relaxation processes and contributions from conductivity are combined. If the latter has an electronic origin (such as in electrode- or Maxwell-Wagner-Sillars-polarization), it does not contribute to ε' but ε'' is directly proportional to the d.c.-conductivity of the sample (σ_0) and inversely proportional to ω^{-s}, where $s < 1$. In this sense, a secondary power law (PL) function is required to properly fit the complex dielectric function, as shown in equation (5):

$$\varepsilon^*(\omega) = -ia\left(\frac{\sigma_0}{\varepsilon_v\omega^s}\right) + \varepsilon^*_{HN}(\omega) \tag{5}$$

where ε_v is the dielectric permittivity of vacuum (a constant value, $\varepsilon_v = 8.854 \times 10^{-12}$ AsV^{-1}m^{-1}).

2.3.3. Crosslink density

Mooney-Rivlin Method: The stress–strain analysis also allows the calculation of ν in mol cm^{-3}, using the Mooney-Rivlin method [36,37]. For this purpose, the stress (σ) and strain (ε) values obtained from the tensile test (section 2.2.5) were used. Subsequently, the reduced stress (σ_{red}) was plotted as a function of the inverse of the strain ratio (λ^{-1}, with $\lambda = 1 + \varepsilon$) using equation (6):

$$\sigma_{red} = \frac{\sigma}{\lambda - \lambda^{-2}} = 2C_1 + 2C_2\left(\frac{1}{\lambda}\right) \tag{6}$$

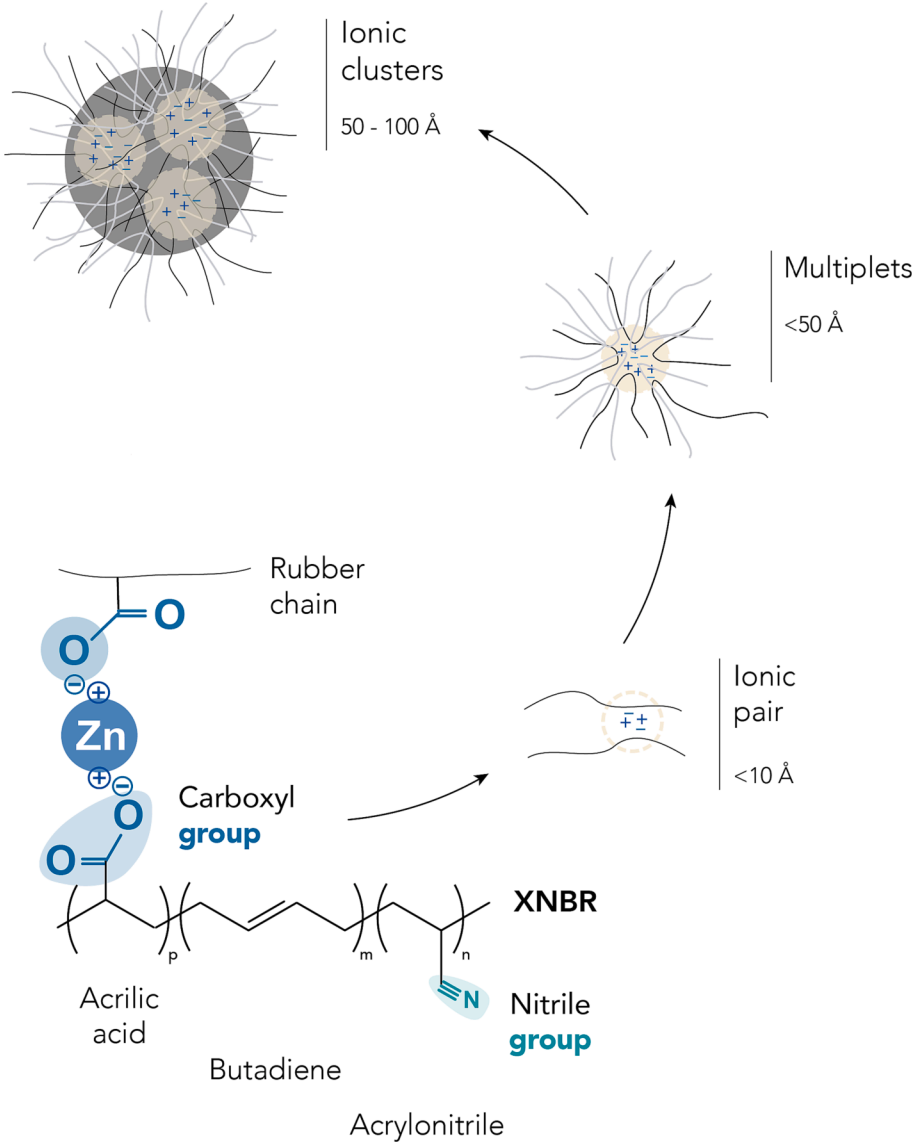

Fig. 4. Scheme of the ionic domains of XNBR/ZnO compounds.

where C_1 represents the contribution of crosslinking units, whereas C_2 denotes the Mooney-Rivlin elastic constant and is related to the trapped entanglements. From the linear region of the plot, the *y*-interception is $2C_1$ and the slope is $2C_2$. Consequently, ν can be calculated by equation (7):

$$2C_1 = N_A \nu k T \tag{7}$$

where N_A is Avogadro's number (6.02×10^{-23} mol^{-1}), k is the Boltzmann's constant (1.38×10^{-23} J/K), and T is the temperature (in K).

Swelling Test: The crosslink density (ν) was calculated following the swelling method in toluene and expressed in mol cm^{-3}. Five samples with a square section of approximately 1 cm × 1 cm × 2 mm were taken. These samples were then immersed in the selected solvent (i.e., toluene) for 72 h at room temperature (RT), extracted, and dried in air until the solvent was evaporated (constant mass). The mass of each sample was recorded before immersion (m_1), after swelling for 72 h (m_2), and after evaporation of the absorbed solvent (m_3). The Flory-Rehner expression considering the affine model and tetra-functional networks, $f = 4$, was required to calculate ν according to equation (8):

$$\nu = -\frac{\ln(1 - V_r) + V_r + \chi V_r^2}{2V_S\left(V_r^{\frac{1}{3}} - \frac{V_r}{2}\right)} \tag{8}$$

where V_S is the molar volume of toluene (106.28 cm^3 mol^{-1}), χ is the Flory-Huggins interaction parameter between XNBR and toluene (calculated using the expression $0.4132 + 0.4341 V_r$ [38]) and V_r is the volume fraction of rubber in the recipe, calculated according to equation (9):

$$V_r = \frac{\frac{m_3}{\rho_r}}{\frac{m_3}{\rho_r} + \frac{m_2 - m_3}{\rho_s}} \tag{9}$$

where ρ_s is the density of toluene (0.867 g cm^{-3}). The reported values for all calculations include the mean and their corresponding standard deviations.

2.3.4. Fourier transform infrared Spectroscopy (FTIR-ATR)

A spectrometer (Spectrum Two, Perkin Elmer) was used to obtain the infrared spectra of the compounds in ATR mode from 400 to 4000 cm^{-1} with a resolution of 4 cm^{-1} and 4 scans per spectrum.

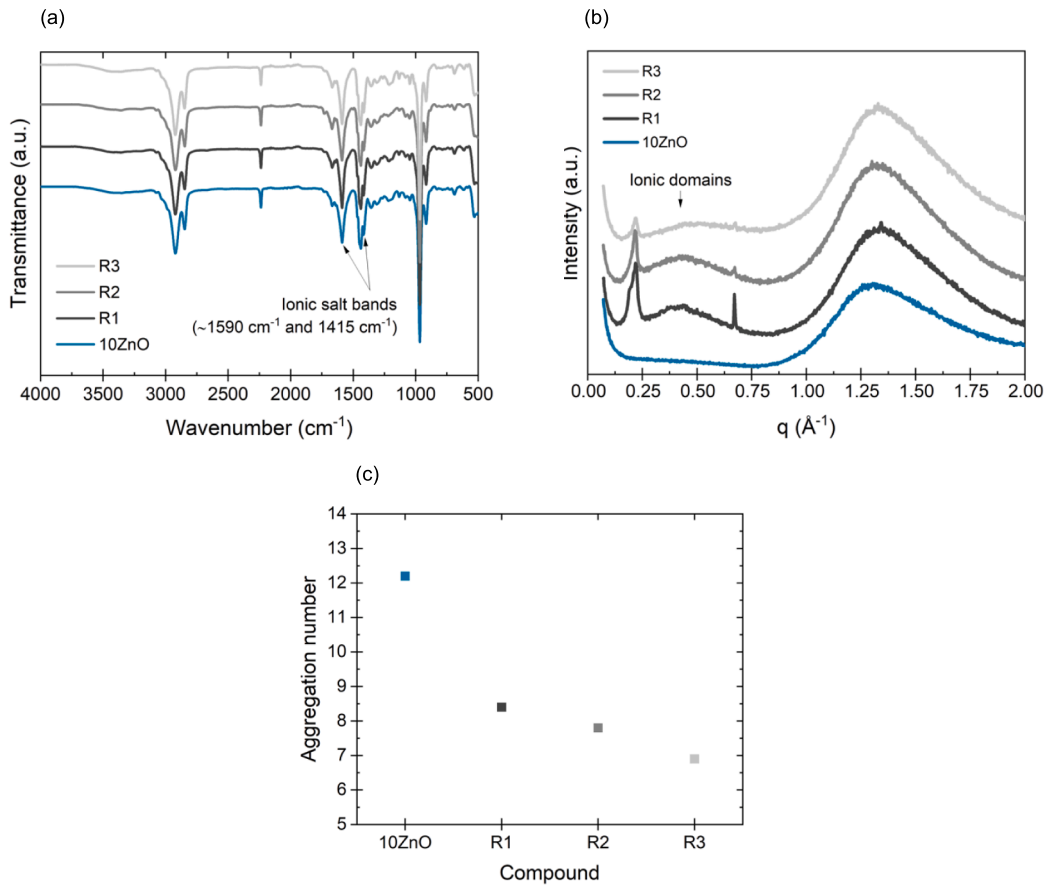

Fig. 5. (a) FTIR-ATR spectra, (b) XRD diffractograms, and (c) aggregation numbers for pristine 10ZnO and recycled samples.

2.3.5. X-ray diffraction (XRD)

A diffractometer (D8 Advance, Bruker) with Cu-K α radiation (with $\lambda = 1.52$ Å) was used to obtain diffraction patterns over a wide 2 θ range between 1° and 90° (WAXS) under standard conditions (0.2 s per step) using vulcanized solid samples of 1–2 mm in thickness.

2.3.6. Scanning electron microscopy (SEM)

Environmental SEM (XL30, Phillips) was used to observe the morphological changes during the recycling cycles. The microscope was equipped with a tungsten filament. An acceleration voltage of 25 kV was fixed. Due to the polymeric character of the samples, the surfaces required sputter coating with a gold alloy. The cross-section resulting from a cryogenic fracture was observed.

2.3.7. Tensile test

Tensile tests were conducted on dumbbell-shaped specimen type 3, in accordance with the UNE–ISO 37:2013 standard, using a universal testing machine (4204, Instron) equipped with a 50 kN load cell. The tests were performed at an extension rate of 200 mm min^{-1} and an initial gauge length of 35 mm. The tensile strength (TS), elongation at break (EB) (defined as the maximum stress and strain values, respectively), and the "modulus" (stresses) at 100 % (M100), 300 % (M300), and 500 % (M500) elongation were recorded. All reported magnitudes are the mean values of five samples tested and their corresponding standard deviations, while the shown stress–strain curves are the most representative of the mean values.

2.3.8. Cyclic tensile test

Cyclic tensile tests were conducted using the same type of samples and equipment as the tensile tests, but with an extension rate of 500 mm min^{-1} to 300 % strain, up to ten times. To simplify the plots, only the curves of the first three loading and unloading cycles are shown; thereafter, the changes were negligible.

2.3.9. Fatigue test

The compressive fatigue response was studied using a tabletop testing system (858, MTS), employing cylindrical samples with a diameter of 16 mm and height of 12.5 mm. Sinusoidal oscillation with an amplitude of 3.1 mm (25 % compressive strain) at 10 Hz frequency were set. All experiments were carried out up to 10,000 cycles at RT. The final height of the samples was recorded after 5 min and 30 days.

2.3.10. Chemical resistance

To evaluate the chemical resistance of the prepared recipes, five samples (1 cm × 1 cm × 2 mm) were immersed in three non-polar solvents (toluene, gasoline, and motor oil) for 72 h at RT. Before (m_i) and after (m_f) immersion, the samples were weighed to determine the mass change (Δm, %), which was used as an indirect measure of the chemical resistance, calculated according to equation (10):

$$\Delta m = 100\frac{m_f - m_i}{m_i} \tag{10}$$

3. Results and discussion

The first step was to identify the structure of the rubber network using DMA. Supporting Information S1 shows the temperature-dependent behavior of storage (E') and loss modulus (E'') for the selected system before and after each recycling cycle (R1, R2, and R3), respectively. The E' values exhibit two clear drops, one near 0 °C and a smaller one between 25 and 50 °C. Meanwhile, the E'' curve displays

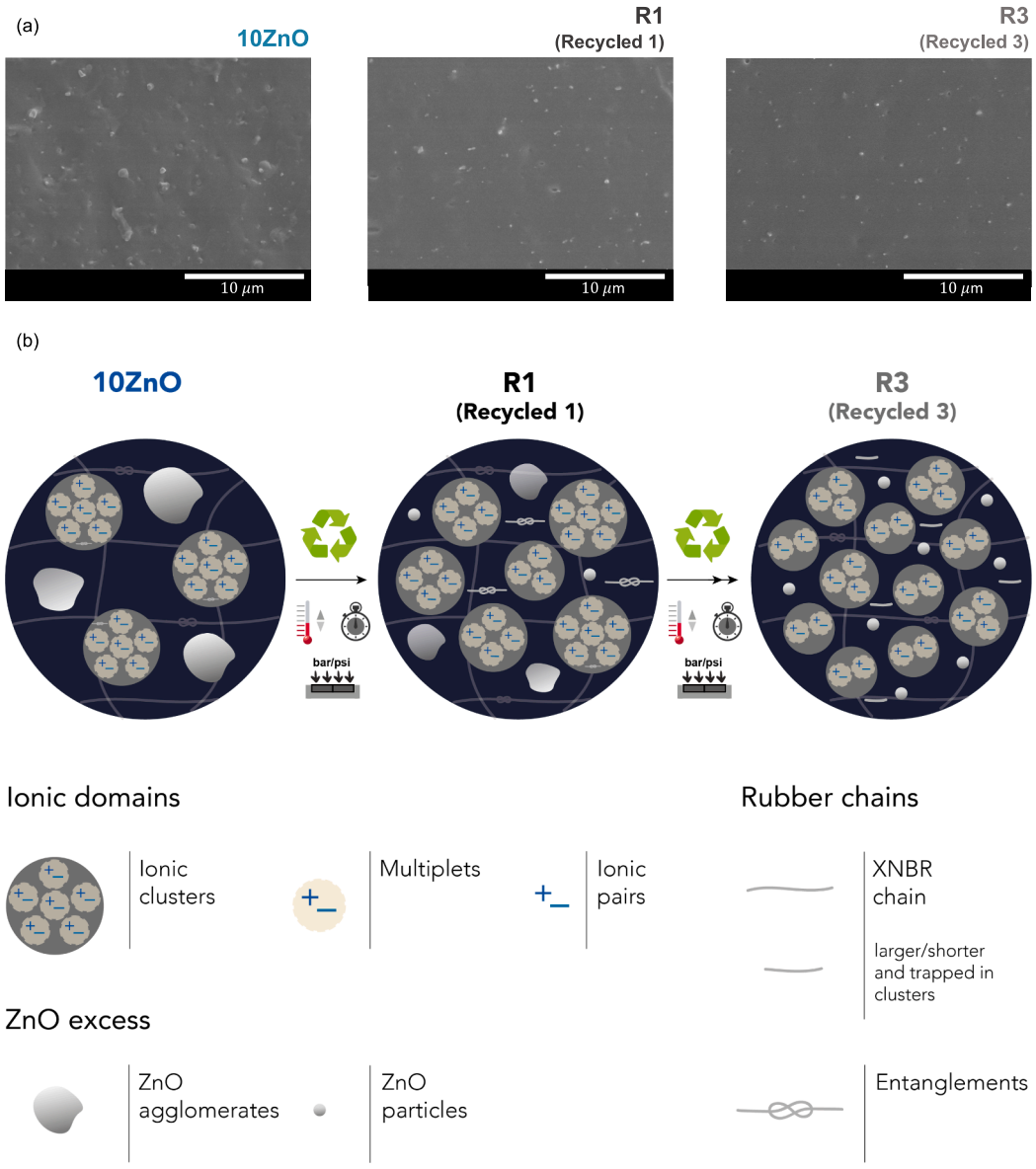

Fig. 6. (a) 10ZnO, R1 and R3 photomicrographs by SEM. (b) Schematic representation of the molecular changes through the recycling cycles.

another broader and more diffuse peak at lower temperatures around −35 °C, indicating the presence of a third thermally activated process. To verify the nature of these zones, the $\tan(\delta)$ values were plotted (Fig. 2a), confirming the existence of three relaxation processes designated as β, α, and α' in all samples. The first relaxation, β, is believed to be associated with short-range non-cooperative motions, but its full nature is still unclear, despite some attempts to explain its origin in non-carboxylated acrylonitrile-butadiene rubber (NBR) with a different vulcanization agent ($ZnCl_2$) [39]. The second, α, is related to the segmental motions of the material during glass transition. The third, α', is the ionic relaxation, due to the chemical nature of the characteristic ionic domains, present in this type of elastomer. The nature of the latter two relaxations (α and α') has been previously reported in the scientific literature [14], where it was also demonstrated that not all kind of ionic linkages or coordination complexes contribute to the manifestation of the high-temperature relaxation phenomenon (above glass transition). This is observed only when ionic linkages contribute to the formation of clusters, that is, the formation of a hard phase with its own glass/ionic transition [12].

With the recycling cycles, the α relaxation exhibits a decrease in the intensity of $\tan(\delta)$, which is probably related to an increase in the elastic component of the material, and a shift towards higher temperatures. This behavior can be attributed to an increase in crosslink density during recycling. The α' relaxation remained unchanged in intensity but shifts towards higher temperatures. This trend may suggest a more restricted mobility in the vicinity of the ionic domains, possibly due to changes in the morphology of multiplets and clusters with the cycles. To gain further insights, this analysis was complemented with BDS. Fig. 2b and 2c show the behavior of ε'' and M'' as functions of the temperature. The results observed by BDS confirm the presence of the three characteristic relaxations in the XNBR/ZnO system, both in the pristine sample and in each recycled sample. In addition, they corroborate the shift towards higher temperatures of α and α' relaxation with the cycles (see inset in Fig. 2d).

To shed light on the underlying molecular dynamics of each relaxation, the values of ε'' were studied over a wide range of frequencies. Fig. 3a, 3b and 3c show the three relaxations β, α and α' at selected temperatures, −30, 0 and 15 °C, where they are well resolved in R1 for illustrative purposes. The fitting of the relaxations in the pristine and recycled compounds was performed using HN-functions (see Supporting Information S2). In addition, because of the ionic character of the

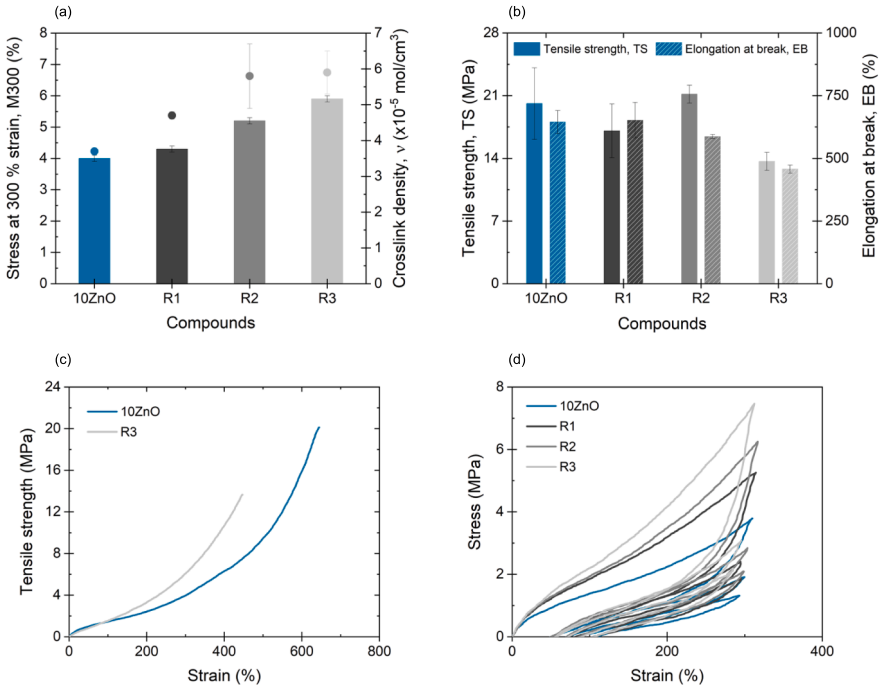

Fig. 7. (a) Stress at 300 % elongation, M300 and crosslink density, (b) Tensile strength, TS and elongation at break, EB and (c) Stress–strain curves of pristine 10ZnO and recycled samples. (d) Cyclic tensile curves at 300 % strain.

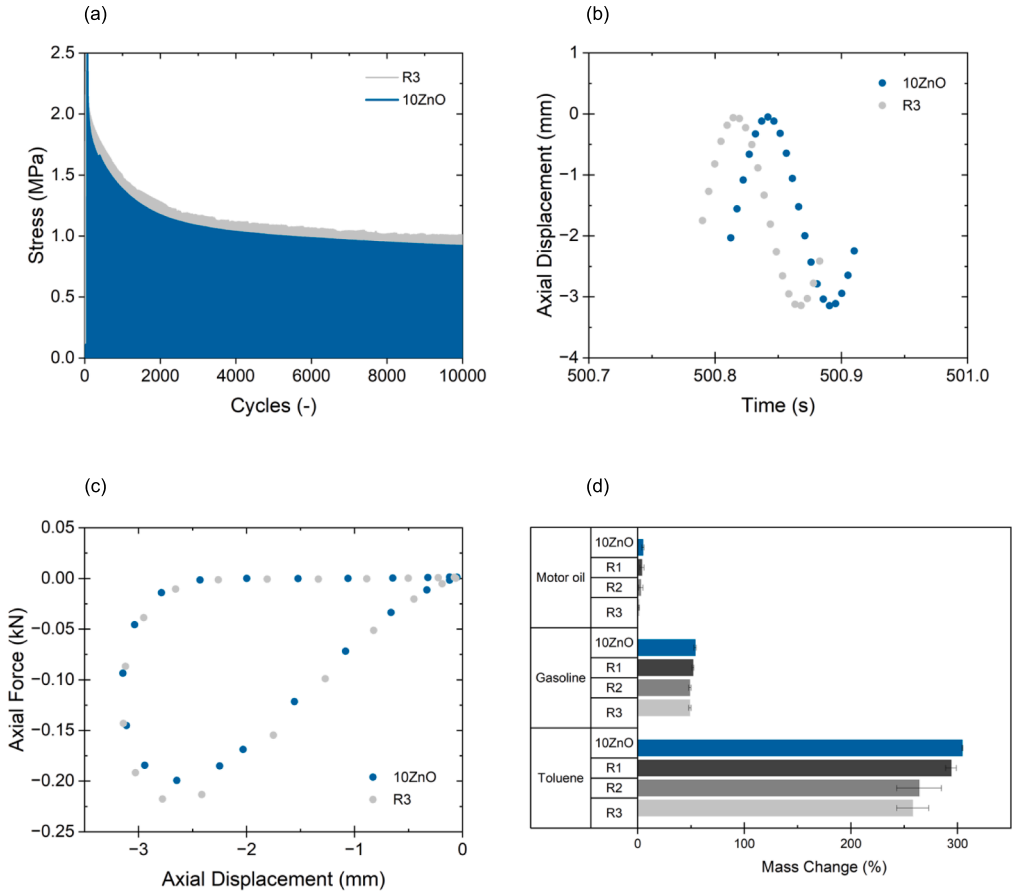

Fig. 8. (a) Stress vs compressive fatigue cycles, (b) axial force vs axial displacement for 5000th loading and unloading cycle and (c) axial displacement vs time for 10ZnO and R3. (d) Mass change in different non-polar solvent as an indirect measure of the chemical resistance of 10ZnO and recycled samples.

samples, the effects of high conductivity above the glass transition were combined with α' relaxation, requiring the use of an additional component, in the form of a PL-function, for a proper fitting of ε'', as suggested in the experimental section.

The activation diagram of the studied samples (Fig. 3d) was obtained from the values of τ_{max} of each relaxation. It can be concluded that recycling cycles do not seem to have a considerable influence on β relaxation. This may be related to the local character of these motions, which are not directly affected by the overall elastomeric amorphous phase or by the ionic domains of the material. However, the changes in the main relaxations (α and α') were more evident. To gain deeper insight into the behavior of the material, two mathematical functions were used to fit the activation diagrams, providing further elucidation of the underlying mechanisms governing the relaxation motions. For the α relaxation, a Vogel-Fulcher-Tammann-Hesse (VFTH) function was used according to equation (11):

$$\tau_{max} = \tau_0 \exp\left(\frac{B}{T - T_0}\right) \tag{11}$$

where T_0 is the Vogel temperature and B and τ_0 are empirical parameters with B related to the fragility strength (D), according to equation (12):

$$B = DT_0 \tag{12}$$

The classification of strong or fragile behavior is closely related to the cooperativity of segmental chain movements. Fragile materials are characterized by high cooperativity (typically with rigid backbones) and a marked departure from Arrhenius behavior. Fragility results in low D values and high fragility index (m) values, indicating a greater apparent activation energy required for their molecular motions. Conversely, materials with low cooperativity exhibit the opposite trend, where their molecular dynamics are more easily activated, leading to higher D values and lower m values [40], the latter of which can be estimated by equation (13):

$$m = \left.\frac{\partial \log\tau(T)}{\partial\left(\frac{T_g}{T}\right)}\right|_{T=T_g} = \frac{DT_0T_g}{\ln 10 (T_g - T_0)^2} \approx 16 + \frac{590}{D} \tag{13}$$

The analysis of these two parameters has significant implications for the development and design of polymeric materials with tailored properties, as the cooperativity of segmental chain movements is a crucial factor in determining their mechanical and thermal behavior.

For α' relaxation, an Arrhenius function was used, following equation (14):

$$\tau_{max} = \tau_0 \exp\left(\frac{-E_a}{RT}\right) \tag{14}$$

where E_a is the activation energy and R is the universal gas constant (8.314 $JK^{-1}mol^{-1}$). Table 1 lists all parameters obtained from the fittings in the activation diagram.

The results of the polymer relaxation analysis are quite revealing. While the short-range motions between the dipoles (β relaxation) remained unaffected by the recycling process, the effects on the segmental dynamics (α relaxation) and the ionic relaxation (α' relaxation) were significant. All values obtained showed an initial effect during the first recycling cycle (R1). For α relaxation, the higher values of T_0 and m (lower B and D) reflect an apparent increase in the stiffness of the polymer chains after the first cycle, i.e., a more fragile polymer backbone. The same trend was also observed for α', which reached E_a values of 101 kJ mol^{-1} compared with 85 kJ mol^{-1} for the original sample. However, the subsequent recycling cycles (R2 and R3) reversed this trend in α relaxation. A priori, these results seem to be inconsistent with the shift towards higher temperatures, as seen in the $\tan(\delta)$ values obtained by DMA. However, these results may indicate that factors other than the pure value of the crosslink density can influence the molecular dynamics.

For further analysis, crosslink density values were calculated using the Flory-Rehner and Mooney-Rivlin methods. The latter is particularly useful because it considers two contributions, the first from the chemically crosslinked network product of vulcanization ($\propto 2C_1$); and the second from the intrinsic molecular entanglements between polymer chains ($2C_2$) [41]. Table 2 shows the mean values, and Supporting Information S3 shows the Mooney-Rivlin plot and the data used.

The Flory-Rehner and Mooney-Rivlin results confirmed the increase in crosslink density with recycling cycles, supporting the observations made by DMA. The Mooney-Rivlin values provided further insight into the trends observed by the BDS. The increase in $2C_1$ values with recycling cycles validates the increase in crosslink density, whereas $2C_2$ shows a maximum value after the first recycling cycle (R1). This suggests that during the first stage of recycling, there was a simultaneous increase in the crosslink density and molecular entanglements in the rubber chains, resulting in increased chain rigidity and polymer fragility. However, subsequent cycles led to a decrease in the number of molecular entanglements. This may be due to increased mobility associated with greater exposure to ion-hopping movements and/or chain scission resulting from the continuous cuts made during the recycling protocol, allowing shorter chains (with fewer topological constraints to confine them) to release such entanglements [42]. These results indicate that entanglements and network defects significantly influence the molecular dynamics of the recycled material.

As mentioned above, the invariance of the α' relaxation intensity observed by DMA suggests that the nature of the ion pairs involved in rubber crosslinking (Fig. 4) is the same. This was evidenced by FTIR-ATR (Fig. 5a), where no changes in the bands corresponding to the ionic salts (at 1590 and 1415 cm^{-1}) were observed with the recycling cycles. Nevertheless, the relaxation shift towards higher temperatures suggests some changes in the morphology and aggregation of this restricted region. The XRD diffractograms (Fig. 5b) show a shift in the maximum of the ionic domains' region (q values from 0.1 to 0.7 Å, related to periodic distances between 63 and 9 Å) [43–45] towards higher q values with the recycling cycles. The observed shift, which indicates a reduction in the spacing between multiplets and clusters, may be attributed to a decrease in the size and number of larger aggregates, and a more homogeneous dispersion of the particles throughout the rubber matrix. This results in a loss of electronic contrast, which accounts for the decrease in the scattered intensity [43]. To further illustrate this phenomenon, the aggregation number was estimated, defined as the number of carboxylates (or ionic pairs) associated with ionic interactions. Based on the FTIR results, where the band associated with the carboxyl groups completely disappeared (at ~ 1700 cm^{-1}), it can be assumed that all the groups participated in at least one ionic interaction, given that the matrix was completely saturated. Using the ratio between the concentration of carboxyl groups present in the rubber matrix (1.53×10^{-3} mol cm^{-3}) and the ionic crosslink density obtained by Mooney-Rivlin, the theoretical aggregation number at room temperature was calculated [45]. The results show that the aggregation number decreases with the number of recycling cycles, from 12.2 for 10ZnO to 6.9 in R3 (Fig. 5c), almost by half. This indicates that the number of ion pairs involved in each higher-order structure decreases as a consequence of their redistribution, leading to an increase in the number of smaller aggregates, and hence, the crosslink density.

The SEM micrographs obtained in this study provide compelling evidence highlighting the remarkable effects of recycling on the Zn-based crosslinked XNBR network. Fig. 6a shows the presence of large white dots corresponding to ZnO particles and aggregates that are uniformly distributed in the XNBR matrix in the original compound (10ZnO) and the first (R1) and third (R3) recycling cycle samples. The significant decrease in the number and size of these white dots in R3 indicates that more residual ZnO was converted to Zn^{2+} salt [46]. It is

suggested that the movement of ions with increasing temperature (ion-hopping) frees some carboxylated groups ($R\text{-}COO^-$) and allows the formation of smaller domains distributed throughout the matrix. This is in line with the redistribution of larger clusters and formation of smaller domains, resulting in an increase in the crosslink density and stiffness of the material. These findings provide a pathway for the tunability of recyclable ionically crosslinked XNBR through the control of excess ZnO and/or entanglement (with partial substitution of recycled by virgin material), leading to the development of sustainable materials with improved mechanical properties. Fig. 6b shows a schematic representation of the proposed changes during the recycling cycles.

At this point, various properties of practical interest (i.e., tensile strength, hysteresis, compressive fatigue behavior, and chemical resistance) and their correlation with changes at the molecular level were studied. Fig. 7a and 7b show the results of uniaxial tensile tests (M300, TS, and EB). Starting with the M300 values, it can be seen that the material becomes stronger with the recycling cycles owing to the increased crosslink density and stiffness. In addition, the compound maintained its initial properties (~20 MPa in TS and ~ 645 % in EB) at the breaking point after two cycles (~21 MPa in TS and ~ 590 % in EB). The subsequent decrease in TS and EB (~14 MPa and ~ 460 %, respectively) could be a consequence of the reduction in the molecular entanglements that provide mechanical resistance to rubber, as stated previously. However, although there may be a decrease in TS after multiple recycling cycles, the properties achieved in R3 are still competitive compared to many other available elastomeric matrices and consider only one additional ingredient in the rubber recipe [21,47,48]. It is important to note that even after three cycles, the material did not lose its typical hyperelastic behavior, as shown by the stress–strain curves in Fig. 7c. Hence, the XNBR/ZnO system studied herein can be used in other less mechanically demanding products, thus closing the loop on our resource consumption.

From another point of view, the loss of properties at the breaking point could be compensated for by preparing new blends using the recycled material as a partial replacement for the virgin material. In this way, a compromise between the crosslink density and molecular entanglements could be found, which allows the maintenance of the mechanical behavior at the fracture point during a greater number of recycling cycles.

Hysteresis loops were also performed and the results are shown in Fig. 7d. A well-known phenomenon of stress softening was observed in all cases. Although this phenomenon in gums is still a subject of debate, it is generally accepted that it is due to the breaking of crosslinking points or chains during deformation, or permanent local orientation after recovery [49,50]. The hysteresis loops increased in area as the recycling cycles progressed, suggesting an increase in the crosslink density of the material. This finding reinforces previous observations that the strength of the material (at low and medium strains) can be improved by recycling.

Compressive fatigue tests showed slightly different mechanical responses for the virgin and recycled materials. In particular, stress decay over compression load cycling was observed (Fig. 8a), with a higher stress level for the recycled rubber (approximately 10 %). Moreover, the sinusoidal displacement conditions (Fig. 8b) and measured permanent sets after 5 min (10.40 mm pristine vs 10.55 mm recycled, on average) highlighted the enhanced hysteresis loop after recycling (Fig. 8c) already at 25 % strain level and higher elastic response, respectively. In line with the observations in the cycled tensile mode, these results suggest a higher crosslink density for the recycled material.

The study of chemical resistance is another crucial aspect for ensuring the viability of recycling XNBR, a highly sought-after elastomer, owing to its excellent resistance to petroleum-derived fluids. For this reason, a study of the mass change of XNBR samples after immersion in three non-polar solvents (motor oil, gasoline and toluene) was carried out. The results obtained, as shown in Fig. 8d, reveal an undeniable trend of decreasing mass change as the number of recycling cycles increases, which perfectly correlates with the increase in crosslink density.

These observations provide straightforward evidence of the close relationship between the molecular structure, crosslink density, and mechanical behavior of the material, including its tensile and compressive strengths, as well as other functional properties such as chemical resistance. These results have significant implications for the future development of XNBR materials with improved mechanical properties, increased sustainability, and enhanced chemical resistance, which are essential for widespread industrial applications.

4. Conclusions

This study marks a significant step towards sustainable polymers by understanding the recyclability of XNBR beyond the conventional uniaxial tensile analysis and provides a breakthrough in the well-known field of ionic elastomers. In summary, the results show that XNBR crosslinked with ZnO can be effectively recycled and reused through a simple and easily scalable process involving only two steps: cutting and (re)molding. The feasibility and practicality of this strategy provides a sustainable solution for rubber waste. The benefits of this process include 100 % recycled material to produce new samples (after the first cycle), leaving the door open for further optimization of the recycling methodology through complementary approaches such as the partial substitution of virgin material. Moreover, this study offers valuable insight into the molecular-level changes during each recycling cycle, providing a comprehensive understanding of the overall material properties. The results demonstrate that the uniaxial tensile properties of the developed XNBR/ZnO compound were minimally affected after three recycling cycles; however, this effect was more pronounced during the third cycle, probably owing to a decrease in molecular entanglements in the rubber network, according to the Mooney-Rivlin analysis. However, the material stiffness increases due to a sustained improvement in the crosslink density and a decrease in the size of the ionic domains (higher number of smaller ionic aggregates), causing restricted molecular dynamics in the vicinity of the ionic phase, as demonstrated by DMA, BDS, and XRD. The trade-off between molecular dynamics and entanglements allows the material to maintain its overall behavior, even under compressive fatigue conditions. These findings suggest that recycling of purely ionically crosslinked XNBR is not only possible but also offers significant advantages in terms of sustainability and performance at room temperature. These results provide a promising avenue for future research and development in this area, ultimately contributing to a more Circular Economy.

CRediT authorship contribution statement

Saul Utrera-Barrios: Conceptualization, Methodology, Formal analysis, Investigation, Data curation, Writing – original draft, Writing – review & editing, Visualization, Supervision. **Reyes Verdugo Manzanares:** Methodology, Validation, Formal analysis, Investigation, Data curation. **Antonio Mattia Grande:** Methodology, Formal analysis, Investigation, Data curation, Writing – review & editing. **Raquel Verdejo:** Conceptualization, Writing – review & editing, Visualization, Project administration, Funding acquisition. **Miguel Ángel López-Manchado:** Conceptualization, Writing – review & editing, Visualization. **Marianella Hernández Santana:** Conceptualization, Formal analysis, Resources, Data curation, Writing – review & editing, Visualization, Supervision, Project administration, Funding acquisition.

Declaration of Competing Interest

The authors declare that they have no known competing financial interests or personal relationships that could have appeared to influence the work reported in this paper.

Data availability

Data will be made available on request.

Acknowledgements

The authors acknowledge the State Research Agency of Spain (AEI) for a research contract (PID2019-107501RB-I00/AEI/10.13039/501100011033) and M. Hernández Santana for a Ramón y Cajal contract (RYC-2017-22837). S. Utrera-Barrios acknowledges the Spanish National Research Council (CSIC) for a predoctoral contract (PIE-202060E183). R. Verdugo Manzanares acknowledges the Community of Madrid for a research assistant contract (PEJ-2019-AI/IND-1635). All authors also acknowledge *Arlanxeo* for kindly providing XNBR and PTI + SusPlast from CSIC for their support.

Appendix A. Supplementary data

S1. E' and E'' vs temperature by DMA; S2. HN- (dash) and PL-function (dots) fittings for (a) β, (b) α and (c) α' relaxations for pristine and recycled compounds; S3. Mooney-Rivlin plot and data. Supplementary data to this article can be found online at https://doi.org/10.1016/j.matdes.2023.112273.

References

[1] H.P. Brown, Carboxylic Elastomers, Rubber Chem. Technol. 30 (1957) 1347–1386, https://doi.org/10.5254/1.3542762.
[2] L. Ibarra, A. Rodríguez, I. Mora-Barrantes, Crosslinking of Unfilled Carboxylated Nitrile Rubber with Different Systems: Influence on Properties, J. Appl. Polym. Sci. 108 (4) (2008) 2197–2205.
[3] J.A. Brydson, Rubbery Materials and Their Compounds, London and New York, Elsevier Applied Sciences, 1988.
[4] L. Ibarra, The Effect of Crosslinking Type on the Physical Properties of Carboxylated Acrylonitrile Butadiene Elastomers, J. Appl. Polym. Sci. 73 (1999) 927–933, https://doi.org/10.1002/(SICI)1097-4628(19990808)73:6.
[5] L. Ibarra, M. Alzorriz, Ionic Elastomers Based on Carboxylated Nitrile Rubber and Magnesium Oxide, J. Appl. Polym. Sci. 103 (2007) 1894–1899, https://doi.org/10.1002/APP.25411.
[6] L. Ibarra, M. Alzorriz, Ionic Elastomers Based on Carboxylated Nitrile Rubber and Calcium Oxide, J. Appl. Polym. Sci. 87 (5) (2003) 805–813.
[7] L. Ibarra, A. Rodríguez, I. Mora-Barrantes, Crosslinking of Carboxylated Nitrile Rubber (XNBR) Induced by Coordination with Anhydrous Copper Sulfate, Polym. Int. 58 (2009) 218–226, https://doi.org/10.1002/PI.2519.
[8] H.P. Brown, Crosslinking Reactions of Carboxylic Elastomers, Rubber Chem. Technol. 36 (1963) 931–962, https://doi.org/10.5254/1.3539642.
[9] A. Eisenberg, Clustering of Ions in Organic Polymers. A Theoretical Approach, Macromolecules 3 (1970) 147–154, https://doi.org/10.1021/ma60014a006.
[10] A. Eisenberg, B. Hird, R.B. Moore, A New Multiplet-Cluster Model for the Morphology of Random Ionomers, Macromolecules 23 (1990) 4098–4107, https://doi.org/10.1021/ma00220a012.
[11] Ibarra, L.; Alzorriz, M. Vulcanization of Carboxylated Nitrile Rubber (XNBR) by Zinc Peroxide. *Polym Int* **1999**, *48*, doi:10.1002/(SICI)1097-0126(199907)48:7<580::AID-PI186>3.0.CO;2-4.
[12] S. Utrera-Barrios, R.V. Manzanares, J. Araujo-Morera, S. González, R. Verdejo, M.Á. López-Manchado, M.H. Santana, Understanding the Molecular Dynamics of Dual Crosslinked Networks by Dielectric Spectroscopy, Polymers (Basel) 13 (2021) 3234, https://doi.org/10.3390/polym13193234.
[13] F. Tian, Y. Ohki, Charge Transport and Electrode Polarization in Epoxy Resin at High Temperatures, J. Phys. D Appl. Phys. 47 (4) (2014) 045311.
[14] D. Basu, A. Das, K.W. Stöckelhuber, D. Jehnichen, P. Formanek, E. Sarlin, J. Vuorinen, G. Heinrich, Evidence for an in Situ Developed Polymer Phase in Ionic Elastomers, Macromolecules 47 (2014) 3436–3450, https://doi.org/10.1021/ma500240v.
[15] L. Ibarra, A. Marcos-Fernández, M. Alzorriz, Mechanistic approach to the curing of carboxylated nitrile rubber (XNBR) by zinc peroxide/zinc oxide, Polymer 43 (5) (2002) 1649–1655.
[16] D.D. Fleischmann, S. Ayalur-Karunakaran, F. Arbeiter, R. Schaller, A. Holzner, W. Kern, S. Schlögl, Influence of Crosslinker and Water on Mechanical Properties of Carboxylated Nitrile Butadiene Rubber (XNBR), Polym. Test. 66 (2018) 24–31, https://doi.org/10.1016/J.POLYMERTESTING.2018.01.001.
[17] I. Mora-Barrantes, M.A. Malmierca, J.L. Valentin, A. Rodriguez, L. Ibarra, Effect of Covalent Cross-Links on the Network Structure of Thermo-Reversible Ionic Elastomers, Soft Matter 8 (2012) 5201–5213, https://doi.org/10.1039/c2sm06975j.
[18] K. Roy, S.C. Debnath, A. Pongwisuthiruchte, P. Potiyaraj, Review on the Conceptual Design of Self-Healable Nitrile Rubber Composites. 6, 15, 2021, 9975-9981.
[19] J. Jose, A. Nag, G.B. Nando, Processing and Characterization of Recycled Polypropylene and Acrylonitrile Butadiene Rubber Blends, J. Polym. Environ. 18 (2010) 155–166, https://doi.org/10.1007/s10924-010-0195-y.
[20] S. Saiwari, B. Yusoh, A. Thitithammawong, Recycled Rubber from Waste of Natural Rubber Gloves Blending with Polypropylene for Preparation of Thermoplastic Vulcanizates Compatibilized by Maleic Anhydride, J. Polym. Environ. 27 (2019) 1141–1149, https://doi.org/10.1007/s10924-019-01413-2.
[21] L. Imbernon, S. Norvez, From Landfilling to Vitrimer Chemistry in Rubber Life Cycle, Eur. Polym. J. 82 (2016) 347–376.
[22] J. Ekeocha, C. Ellingford, M. Pan, A.M. Wemyss, C. Bowen, C. Wan, Challenges and Opportunities of Self-Healing Polymers and Devices for Extreme and Hostile Environments, Adv. Mater. 33 (2021) 2008052, https://doi.org/10.1002/ADMA.202008052.
[23] B. Zhang, N. De Alwis Watuthanthrige, S.V. Wanasinghe, S. Averick, D. Konkolewicz, Complementary Dynamic Chemistries for Multifunctional Polymeric Materials, Adv. Funct. Mater. 32 (2022) 2108431, https://doi.org/10.1002/ADFM.202108431.
[24] M. Das, R. Parathodika, P. Maji, K. Naskar, Dynamic Chemistry: The next Generation Platform for Various Elastomers and Their Mechanical Properties with Self-Healing Performance, Eur. Polym. J. 186 (2023), 111844, https://doi.org/10.1016/j.eurpolymj.2023.111844.
[25] M. Das, K. Naskar, Development, Characterization and Applications of a Unique Self-Healable Elastomer: Exploring a Facile Metal-Ligand Interaction, Polymer (Guildf) 237 (2021), 124373, https://doi.org/10.1016/J.POLYMER.2021.124373.
[26] M.H. Zainol, Z.M. Ariff, M.F. Omar, T.M. Ping, R.K. Shuib, Self-Healable and Recyclable Nitrile Rubber Based on Thermoreversible Ionic Crosslink Network, J. Appl. Polym. Sci. 139 (2022), https://doi.org/10.1002/APP.51948.
[27] T. Chatterjee, S. Hait, A.B. Bhattacharya, A. Das, S. Wiessner, K. Naskar, Zinc Salts Induced Ionomeric Thermoplastic Elastomers Based on XNBR and PA12, Polymer-Plastics Technol. Mater. 59 (2019) 141–153, https://doi.org/10.1080/25740881.2019.1625389.
[28] S. Salaeh, A. Das, S. Wießner, Design and Fabrication of Thermoplastic Elastomer with Ionic Network: A Strategy for Good Performance and Shape Memory Capability, Polymer (Guildf) 223 (2021), 123699, https://doi.org/10.1016/J.POLYMER.2021.123699.
[29] M. Das, T.K. Sreethu, S. Pal, K. Naskar, Biologically Derived Metal-Cysteine Coordination Complexes Crosslink Carboxylated Nitrile Rubber and Enable Room Temperature Self-Healing, Stretchability, and Recyclability, ACS Appl Polym Mater 4 (2022) 6414–6425, https://doi.org/10.1021/ACSAPM.2C00840.
[30] M.A. Malmierca, A. González-Jiménez, I. Mora-Barrantes, P. Posadas, A. Rodríguez, L. Ibarra, A. Nogales, K. Saalwächter, J.L. Valentín, Characterization of Network Structure and Chain Dynamics of Elastomeric Ionomers by Means of 1H Low-Field NMR, Macromolecules 47 (16) (2014) 5655–5667.
[31] P. Vislavath, S. Billa, S. Praveen, J. Bahadur, K. Sudarshan, T.U. Patro, S.K. Rath, D. Ratna, Heterogeneous Coordination Environment and Unusual Self-Assembly of Ionic Aggregates in a Model Ionomeric Elastomer: Effect of Curative Systems, Macromolecules 55 (2022) 6739–6749, https://doi.org/10.1021/ACS.MACROMOL.2C00784.
[32] S. Utrera-Barrios, J. Araujo-Morera, Pulido de Los, L. Reyes, R. Verdugo Manzanares, R. Verdejo, M.Á. López-Manchado, M. Hernández Santana, An Effective and Sustainable Approach for Achieving Self-Healing in Nitrile Rubber, Eur. Polym. J. 139 (2020), https://doi.org/10.1016/j.eurpolymj.2020.110032.
[33] Y. Ikeda, K. Miyaji, T. Ohashi, T. Nakajima, P. Junkong, VULCANIZATION FOR REINFORCEMENT OF RUBBER, Rubber Chem. Technol. 95 (2022) 161–174, https://doi.org/10.5254/RCT.22.77939.
[34] A. Schönhals, F. Kremer, in: Broadband Dielectric Spectroscopy, Springer Berlin Heidelberg, Berlin, Heidelberg, 2003, pp. 1–33.
[35] A. Schönhals, F. Kremer, in: Broadband Dielectric Spectroscopy, Springer Berlin Heidelberg, Berlin, Heidelberg, 2003, pp. 59–98.
[36] M.A. Mooney, Theory of Large Elastic Deformation. *J Appl Phys* **1940**, *11*, doi: 10.1063/1.1712836.
[37] R.S. Rivlin, D. Saunders, Large Elastic Deformations of Isotropic Materials VII. Experiments on the Deformation of Rubber, Philosoph. Trans. Royal Soc. London Ser. A, Mathemat. Phys. Sci. 243 (1951) 251–288, https://doi.org/10.1098/rsta.1951.0004.
[38] M. Gaca, J. Pietrasik, M. Zaborski, L. Okrasa, G. Boiteux, O. Gain, Effect of Zinc Oxide Modified Silica Particles on the Molecular Dynamics of Carboxylated Acrylonitrile-Butadiene Rubber Composites, Polymers (Basel) 9 (2017) 645, https://doi.org/10.3390/POLYM9120645.
[39] D. Basu, S.S. Banerjee, S. Chandra Debnath, M. Malanin, L. Amirova, P. Dubois, G. Heinrich, A. Das, Unusual Low Temperature Relaxation Behavior of Crosslinked Acrylonitrile-Butadiene Co-Polymer, Polymer (Guildf) 212 (2021), 123309, https://doi.org/10.1016/j.polymer.2020.123309.
[40] A. Sanz, A. Nogales, T.A. Ezquerra, Influence of Fragility on Polymer Cold Crystallization, Macromolecules 43 (2010) 29–32, https://doi.org/10.1021/ma902289k.
[41] M. Gruendken, A. Blume, Network Formation of Low Molecular Weight 'Liquid' Polymers Studied by Gel Permeation Chromatography and Stress-Strain Analysis According to Mooney-Rivlin, Polym. Test. 118 (2023), 107897, https://doi.org/10.1016/J.POLYMERTESTING.2022.107897.
[42] J.L. Valentín, P. Posadas, A. Fernández-Torres, M.A. Malmierca, L. González, W. Chassé, K. Saalwächter, Inhomogeneities and Chain Dynamics in Diene Rubbers Vulcanized with Different Cure Systems, Macromolecules 43 (2010) 4210–4222, https://doi.org/10.1021/ma1003437.
[43] C.X. Sun, M.A.J. Van Der Mee, J.G.P. Goossens, M. Van Duin, Thermoreversible Cross-Linking of Maleated Ethylene/Propylene Copolymers Using Hydrogen-

Bonding and Ionic Interactions, Macromolecules 39 (2006) 3441–3449, https://doi.org/10.1021/ma052691v.
[44] A. Mordvinkin, M. Suckow, F. Böhme, R.H. Colby, C. Creton, K. Saalwächter, Hierarchical Sticker and Sticky Chain Dynamics in Self-Healing Butyl Rubber Ionomers, Macromolecules 52 (2019) 4169–4184, https://doi.org/10.1021/acs.macromol.9b00159.
[45] M. Alonso Malmierca, Elastómeros Iónicos Con Memoria de Forma: Estructura, Dinámica y Propiedades. Tesis doctoral, Universidad Complutense de Madrid, Madrid, 2013.
[46] C. Xu, X. Huang, C. Li, Y. Chen, B. Lin, X. Liang, Design of "Zn2+ Salt-Bondings" Cross-Linked Carboxylated Styrene Butadiene Rubber with Reprocessing and Recycling Ability via Rearrangements of Ionic Cross-Linkings, ACS Sustain. Chem. Eng. 4 (2016) 6981–6990, https://doi.org/10.1021/acssuschemeng.6b01897.
[47] A.M. Wemyss, C. Bowen, C. Plesse, C. Vancaeyzeele, G.T.M. Nguyen, F. Vidal, C. Wan, Dynamic Crosslinked Rubbers for a Green Future: A Material Perspective, Mater. Sci. Eng. R. Rep. 141 (2020), 100561, https://doi.org/10.1016/j.mser.2020.100561.
[48] S. Utrera-Barrios, R. Verdejo, M. López-Manchado, M. Hernández Santana, Self-Healing Elastomers: A Sustainable Solution for Automotive Applications, *Eur. Polym. J.* (2023) 112023, https://doi.org/10.1016/J.EURPOLYMJ.2023.112023.
[49] J. Diani, B. Fayolle, P. Gilormini, A Review on the Mullins Effect, Eur. Polym. J. 45 (2009) 601–612, https://doi.org/10.1016/J.EURPOLYMJ.2008.11.017.
[50] Z. Li, H. Xu, X. Xia, Y. Song, Q. Zheng, Energy Dissipation Accompanying Mullins Effect of Nitrile Butadiene Rubber/Carbon Black Nanocomposites, Polymer (Guildf) 171 (2019) 106–114, https://doi.org/10.1016/J.POLYMER.2019.03.043.